

***Pinus nigra* barks from a mercury mining district studied with high resolution XANES spectroscopy**

Fabrizio Bardelli^{1,2}, Valentina Rimondi³, Pierfranco Lattanzi⁴, Mauro Rovezzi⁵, Marie-Pierre Isaure⁶, Andrea Giaccherini³, Pilario Costagliola³

¹Università di Roma La Sapienza, Roma, Italy; fabrizio.bardelli@gmail.com;

²CNR-Nanote; Italy;

³Università di Firenze, Italy; pilario.costagliola@unifi.it; andrea.giaccherini@gmail.com;

valentina.rimondi@unifi.it

⁴CNR, IGG, Italy; pierfrancolattanzi@gmail.com

⁵Univ. Grenoble Alpes, CNRS, IRD, Irstea, Météo France, OSUG, FAME, Grenoble, France;

mauro.rovezzi@esrf.eu

⁶Université de Pau et des Pays de l'Adour, E2S UPPA, CNRS, IPREM, Pau, France

marie-pierre.isaure@univ-pau.fr

Supporting Information

Figures S1 – S7

Tables S1 – S3

Details on LCF

References



Figure S1. Photograph of a representative black pine bark sampling. The sampling point is at ~150 cm from the ground.

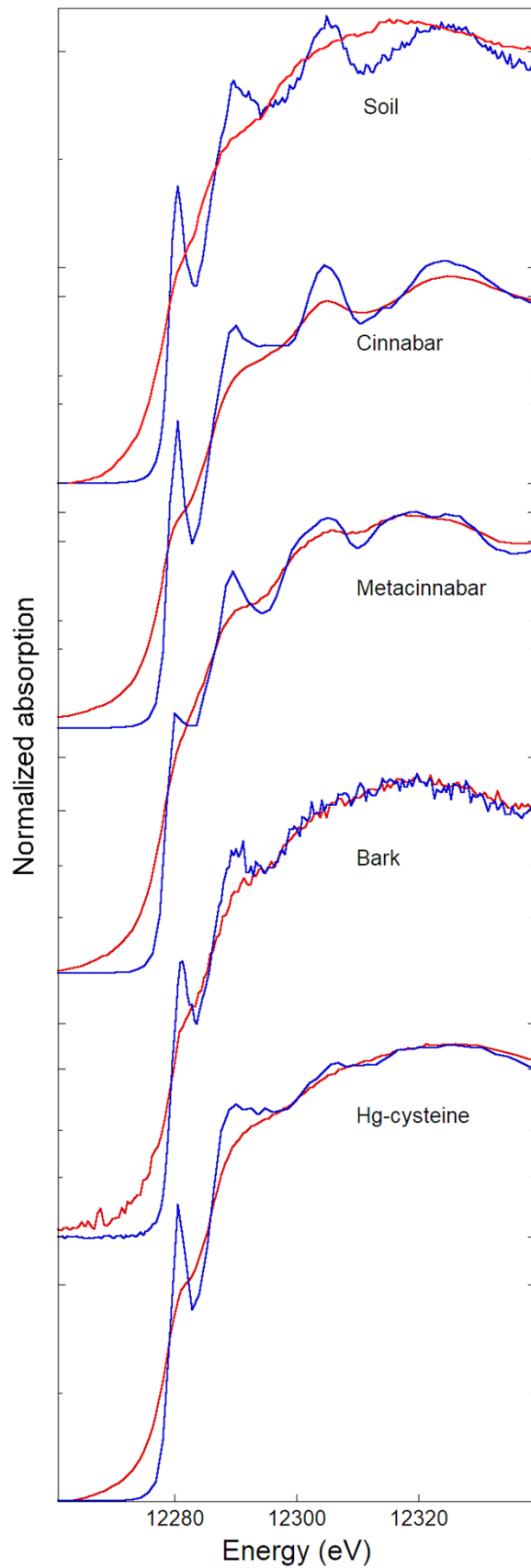


Figure S2. Representative spectra of soil and bark samples, and of organic ($\text{Hg}(\text{Cys})_2$) and inorganic (α - and β - HgS) Hg references acquired with HR-XANES (blue lines) and conventional XANES (red lines). It is evident that high-resolution spectra have more structured features. Conversely, the spectral features of conventional XAS spectra appear largely smeared-out. Richer spectral features allow for easier finger-print analysis or more reliable LCF with reference spectra.

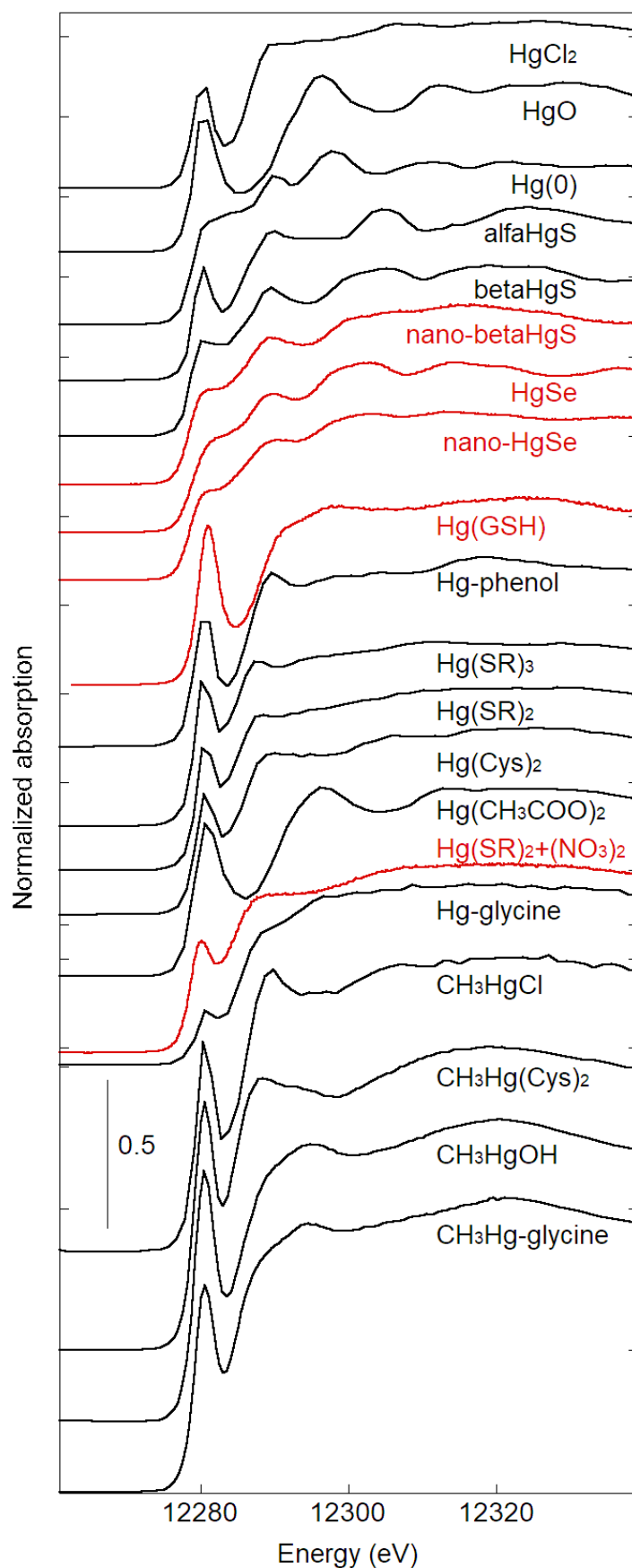


Figure S3. HR-XANES spectra of all Hg reference compounds considered in this study (top: inorganic Hg species; middle: organic Hg species; bottom: methylated Hg species). The spectra were vertically shifted for clarity. The spectra indicated with the red color were obtained from the Supporting Information of the works of Manceau and collaborators (Manceau et al., 2021, 2015) and Bourdineaud and collaborators (Bourdineaud et al., 2019).

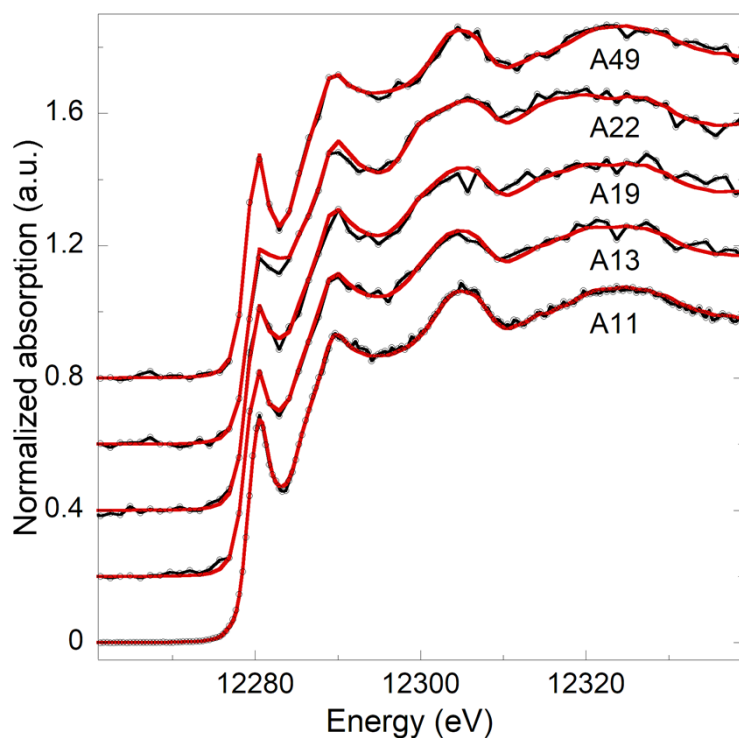


Figure S4. HR-XANES spectra and corresponding LCF curves of soil samples. LCF were performed using the β -HgS and α -HgS references (Table S2).

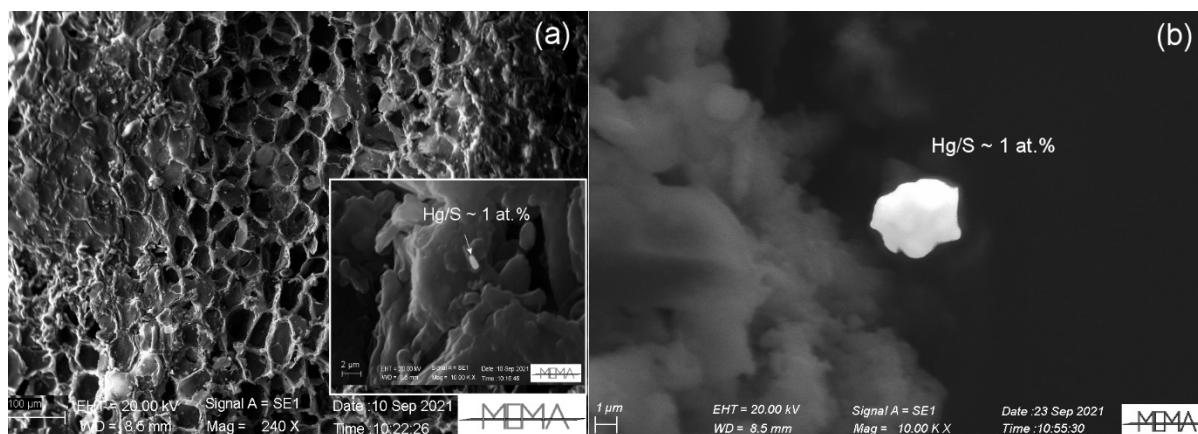


Figure S5. Mixed backscattered and secondary electron images (SEM) of discrete Hg particles of: a) an outer barks layer (sample A13 0-2 mm); b) a soil (sample A11). The Hg to S atomic % ratio from EDS analysis is also shown.

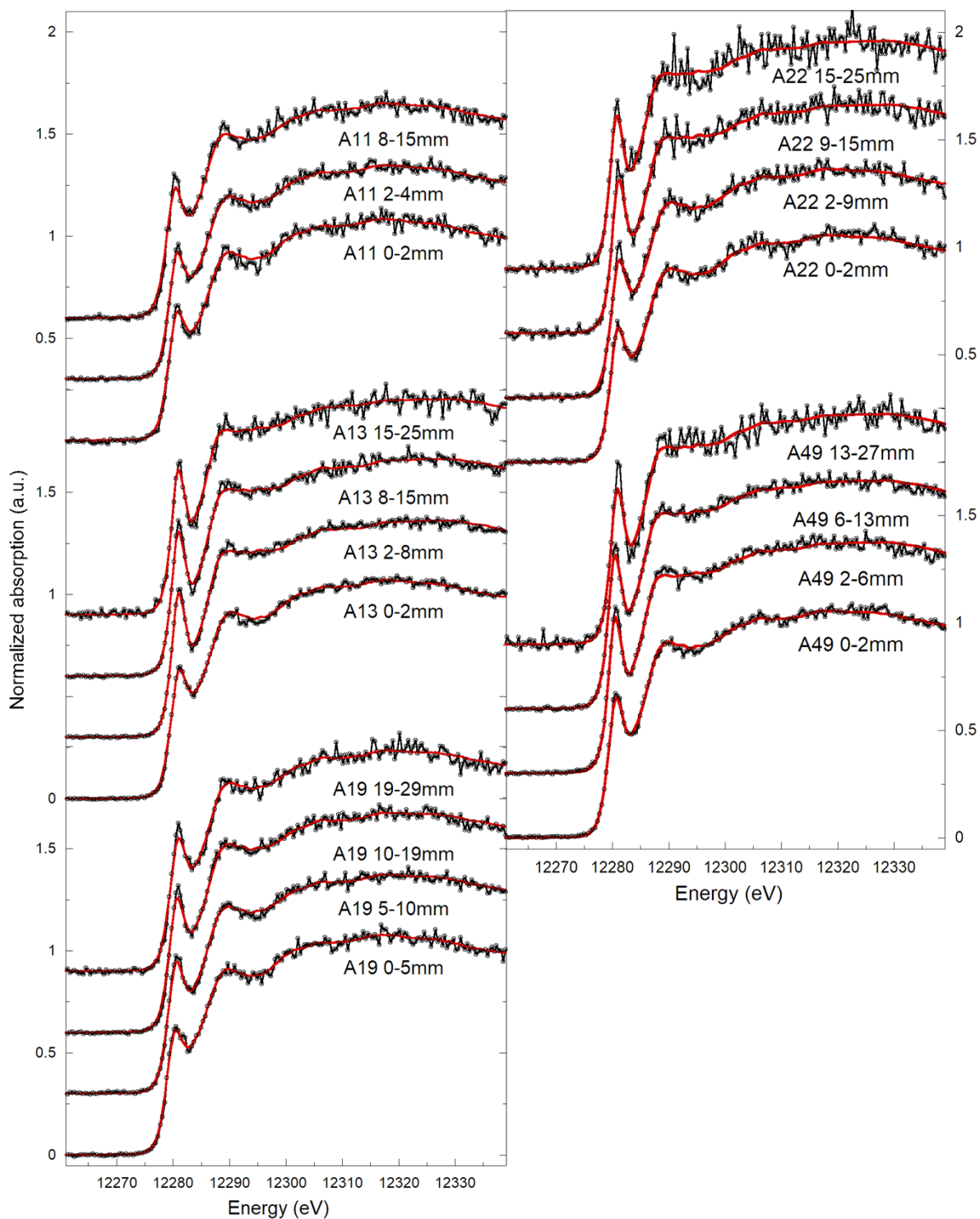


Figure S6. HR-XANES spectra of the bark samples collected at different depth from the bark interface with the atmosphere (lines + points). The continuous red lines represent the LCF curves, which numerical results are reported in table S1.

Table S1. Mercury speciation (%) of all the bark samples as determined from LCF. The numbers between parentheses represent the error on the values as obtained from the minimization software (IFEFFIT - (Ravel, 2001)). The reduced chi-square and the sum of the fractions are also shown.

Sample	Depth mm	nano- β -HgS %	Hg(cys) ₂ %	Hg(SR) ₂ %	Σ	χ^2 ($\times 10^4$)
A11	0 – 2	56(4)	45(4)		101	7.6
	2 – 4	53(3)	45(3)		98	3.8
	4 – 8	40(4)	59(4)		99	7.4
A13	0 – 2	50(3)	50(3)		100	3.1
	2 – 8		76(5)	25(5)	101	4.5
	8 – 15		76(7)	24(7)	101	4.7
	15 – 25		52(10)	49(10)	101	10
A19	0 – 5	56(6)	45(6)		100	3.9
	5 – 10	38(7)	64(7)		101	3.3
	10 – 19	31(8)	70(8)		101	3.3
	19 – 29	39(10) ¹	63(10)		102	8.0
A22	0 – 2	39(4)	60(4)		100	6.4
	2 – 9	38(4)	62(4)		100	6.8
	9 – 15		66(12)	36(12)	101	14 ²
	15 – 25		63(17)	38(18)	101	27 ²
A49	0 – 2	27(3)	72(3)		100	2.8
	2 – 6		59(7)	44(7)	103	5.3
	6 – 13		61(7)	41(7)	101	4.4
	13 – 27		64(14)	38(15)	102	19 ²

¹ The value does not follow the general decreasing trend with the layer depth of the Hg-content or β -HgS fraction.

² The quality of the fit is lower because of a significantly lower signal-to-noise ratio.

Table S2. Mercury speciation (%) of all the soil samples as determined from LCF. The numbers between parentheses represent the error on the values as obtained from the minimization software (IFEFFIT - (Ravel, 2001)). The reduced chi-square χ_v^2 and the sum of the fractions (Σ) are shown.

Sample	β -HgS %	α -HgS %	Σ	χ_v^2 ($\times 10^4$)
A13	55(5)	44(5)	99	2.2
A49	28(4)	71(4)	99	2.1
A22	99(5)	0(5)	99	3.2
A19	72(7)	27(7)	99	4.2
A11	32(3)	68(3)	100	0.8

Table S3. Goodness of fit values for target transformation (TT) procedure: χ^2 is the traditional sum of the squared differentials and the SPOIL value is a measure of the match of the transformed spectrum to the target one (0 – 1.5, excellent; 1.5 – 3.0, good; 3.0 – 4.5, fair; 4.5 – 6.0, acceptable; > 6.0, unacceptable (Malinowski, 1977)). The IND function determined from PCA procedure reached a minimum in correspondence of 4 – 5 components, for the bark samples, and 2 components for the soil samples, (see Figure S6). However, as bark samples spectra can be satisfactorily reconstructed using 3 components, the TT procedure for the bark samples was performed with 3 components (2 for the soil samples). The reference were ordered for increasing SPOIL values. References with SPOIL values higher than 3.0 were considered as non-suitable candidates. However, both SPOIL and χ^2 were considered in choosing the best candidates.

Barks (3 components)			Soils (2 components)		
	SPOIL	χ^2		SPOIL	χ^2
β HgS-nano	1.7	0.37	α HgS	1.3	0.09
β HgS	2.1	0.34	β HgS	2.5	0.16
HgSR ₂	2.6	0.30	β HgS-nano	3.1	0.46
Hg(GSH) ₂	2.6	0.54			
CH ₃ Hg-(Cys) ₂	2.7	1.00	HgSe	4.8	1.19
Hg(cys) ₂	2.9	0.18	HgSe-nano	5.8	0.94
CH ₃ HgCl	2.8	0.44	CH ₃ HgCl	9.7	1.34
HgSR ₃	3.0	0.79	Hg(cys) ₂	10	0.94
HgSe	3.6	1.17	HgSR ₂	11	1.28
HgSe-nano	3.6	0.80	Hg-phenol	15	2.47
CH ₃ Hg-glycine	3.4	0.52	HgSR ₃	16	2.17
CH ₃ HgOH	4.2	1.41			
Hg-phenol	4.8	1.28			
α HgS	5.5	1.07			

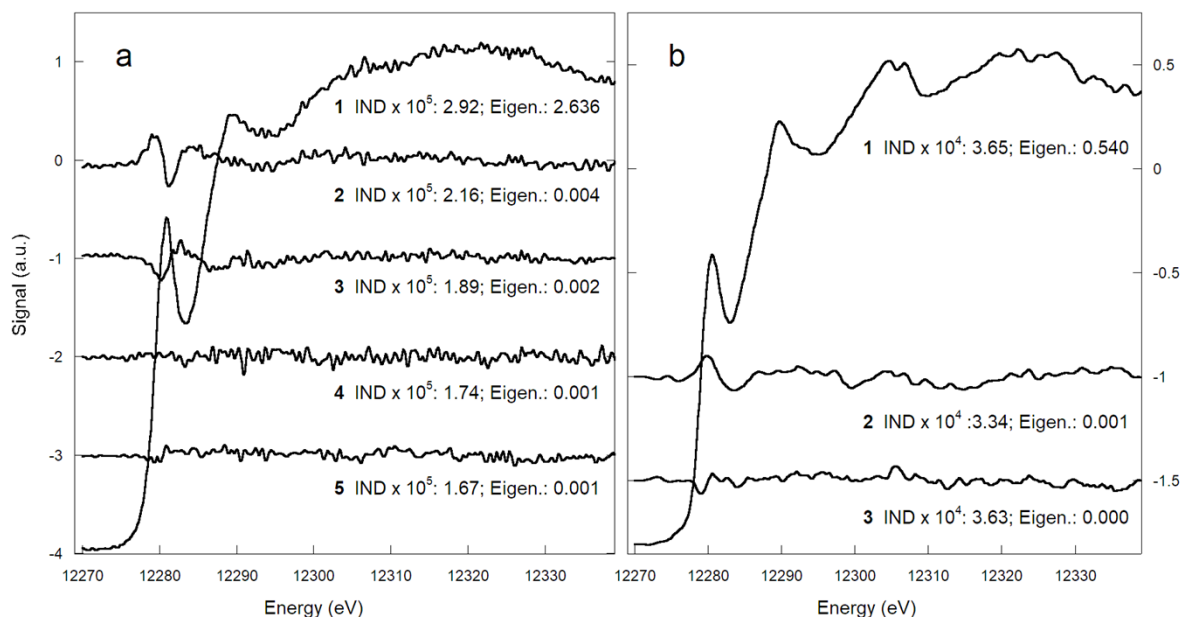


Figure S7. Principal components derived from the nineteen barks spectra (a), and the five soil spectra (b). For the barks spectra, the IND indicator reaches a minimum in correspondence to the 5th component, but it is evident that only the first three components contribute to the signal. For the soil spectra the IND indicator reaches a minimum in correspondence to the 2nd component, and, accordingly, only the first two components contribute to the signal. The eigenvalue (Eigen.) is also reported for each component.

Details on the LCF

The precision of the XANES fractions determined by LCF is difficult to estimate. The errors generated by the fitting software, are to some extent, underestimated because do not consider possible non-optimal choices in the normalization of the XANES spectra, which is somehow arbitrary. Several attempts have been made to establish approaches for the estimation of the errors, but none has become well established (Gustafsson et al., 2020; Manceau et al., 2018). We initially tried to apply the approach described by Manceau et al., 2018, but eventually realized that it was not applicable to our case because our two- and three-component fits resulted in negligible changes in the statistical indicators, suggesting that two-component fits are a better model. Therefore, we used the errors generated by the Athena software (Ravel and Newville, 2005) that we used to perform LCF, which take into account the correlation matrix of the parameters. However, as only two-components were used in LCF, and the energy shifts of the references were kept fixed (after carefully checking the calibration with the Hg(0) reference simultaneously acquired at each scan or the alignment of the references downloaded from published papers (see following), we believe that these errors are not far from the actual uncertainties.

The nanoparticulate β -HgS and Hg(cysteine)₂ (pH7.5) references downloaded from (Bourdineaud et al., 2019) were aligned by matching the beta-HgS reference from the same paper and that of our beta-HgS reference and using the energy shift for the alignment. The HgSe and nanoparticulate HgSe references downloaded from (Manceau et al., 2021) were aligned by matching the nano- β -HgS reference from the same paper and that of nano- β -HgS from the work previously cited and aligned.

Finally, it has to be noted that in noisier spectra (i.e. corresponding to lower Hg concentration/deepest bark layer samples) the difference between the LCF performed with bulk or nano- β -HgS was negligible because the higher noise level hindered the spectral differences above ~ 25 eV.

References

- Bourdineaud, J.P., Gonzalez-Rey, M., Rovezzi, M., Glatzel, Pieter, Nagy, K.L., Manceau, A., 2019. Divalent Mercury in Dissolved Organic Matter Is Bioavailable to Fish and Accumulates as Dithiolate and Tetrathiolate Complexes. *Environ. Sci. Technol.* 53, 4880–4891. https://doi.org/10.1021/ACS.EST.8B06579/SUPPL_FILE/ES8B06579_LIVESLIDES.MP4
- Gustafsson, J.P., Braun, S., Marius Tuyishime, J.R., Adediran, G.A., Warrinnier, R., Hesterberg, D., 2020. A probabilistic approach to phosphorus speciation of soils using p k-edge xanes spectroscopy with linear combination fitting. *Soil Syst.* 4, 1–17. <https://doi.org/10.3390/soilsystems4020026>
- Malinowski, E.R., 1977. Theory of Error in Factor Analysis. *Anal. Chem.* 49, 606–612. <https://doi.org/10.1021/ac50012a026>
- Manceau, A., Bourdineaud, J.P., Oliveira, R.B., Sarrazin, S.L.F., Krabbenhoft, D.P., Eagles-Smith, C.A., Ackerman, J.T., Stewart, A.R., Ward-Deitrich, C., Del Castillo Busto, M.E., Goenaga-Infante, H., Wack, A., Retegan, M., Detlefs, B., Glatzel, P., Bustamante, P., Nagy, K.L., Poulin, B.A., 2021. Demethylation of Methylmercury in Bird, Fish, and Earthworm. *Environ. Sci. Technol.* 55, 1527–1534. https://doi.org/10.1021/ACS.EST.0C04948/ASSET/IMAGES/LARGE/ES0C04948_0006.JPEG
- Manceau, A., Lemouchi, C., Enescu, M., Gaillot, A.-C., Lanson, M., Magnin, V., Glatzel, P., Poulin, B.A., Ryan, J.N., Aiken, G.R., Gautier-Luneau, I., Nagy, K.L., 2015. Formation of Mercury Sulfide from Hg(II)–Thiolate Complexes in Natural Organic Matter. *Environ. Sci. Technol.* 49, 9787–9796. <https://doi.org/10.1021/ACS.EST.5B02522>
- Manceau, A., Wang, J., Rovezzi, M., Glatzel, P., Feng, X., 2018. Biogenesis of Mercury-Sulfur Nanoparticles in Plant Leaves from Atmospheric Gaseous Mercury. *Environ. Sci. Technol.* 52, 3935–3948. <https://doi.org/10.1021/acs.est.7b05452>
- Ravel, B., 2001. ATOMS : crystallography for the X-ray absorption spectroscopist. *J. Synchrotron Radiat.* 8, 314–316. <https://doi.org/10.1107/S090904950001493X>
- Ravel, B., Newville, M., 2005. ATHENA, ARTEMIS, HEPHAESTUS: data analysis for X-ray absorption spectroscopy using IFEFFIT. *J. Synchrotron Radiat.* 12, 537–41. <https://doi.org/10.1107/S0909049505012719>